International Journal of Mechanical, Industrial and Aerospace Sciences
ISSN: 2517-9950
Vol:12, No:12, 2018

Desktop High-Speed Aerodynamics by Shallow Water Analogy in a Tin Box for Engineering Students

Etsuo Morishita

***Abstract*—**In this paper, we show shallow water in a tin box as an analogous simulation tool for high-speed aerodynamics education and research. It is customary that we use a water tank to create shallow water flow. While a flow in a water tank is not necessarily uniform and is sometimes wavy, we can visualize a clear supercritical flow even when we move a body manually in stationary water in a simple shallow tin box. We can visualize a blunt shock wave around a moving circular cylinder together with a shock pattern around a diamond airfoil. Another interesting analogous experiment is a hydrodynamic shock tube with water and tea. We observe the contact surface clearly due to color difference of the two liquids those are invisible in the real gas dynamics experiment. We first revisit the similarities between high-speed aerodynamics and shallow water hydraulics. Several educational and research experiments are then introduced for engineering students. Shallow water experiments in a tin box simulate properly the high-speed flows.

***Keywords*—**Aerodynamics compressible flow, gas dynamics, hydraulics, shock wave.

I. Introduction

HIGH-SPEED aerodynamics is analogous to a shallow water flow and there were many experimental researches on the analogy. Shallow water is used because of its simplicity. Shock wave is easily replaced by hydraulic jump. In this paper, we follow the contents of several eminent textbooks on gas dynamics [1]-[9] and apply the shallow water analogy to several high-speed aerodynamic flows in a tin box for engineering students.

The shallow water analogy has its own long history. In this paper, we revisit the supersonic flows around a circular cylinder [10] and diamond airfoil [11]. We primarily focus on the Mach number and the Froude number analogy and the viscous effect is assumed to be negligible although this is not the case in reality [12].

The under expanded nozzle exit flow is modeled by a flow from a pipe into a shallow water. This method also creates a Mach disc pattern in the shallow water [13].

The dam-break problem in hydraulics [14] is the Riemann problem in gas dynamics. We can simulate this hydraulic shock tube by a shallow water in a conventional plastic box [15].

II. High-Speed Aerodynamics Modeled by Shallow Water Hydraulics Revisited

A. Bernoulli's Equation

The energy equation for a compressible flow is given by

$$\frac{1}{2}u^2 + h = h_0 \tag{1}$$

where h is the specific enthalpy, h_0 the specific total enthalpy, and u the velocity.

Bernoulli's equation for a horizontal uniform water flow becomes

$$\frac{1}{2g}u^2 + \frac{p}{\rho g} + z = h_0 \tag{2}$$

where g is the gravitational acceleration, h_0 the total head, p the static pressure, and z the height form the bottom. In hydraulics, h_0 is the specific energy and often represented by the symbol E. Static pressure becomes

$$p = \rho g(h - z) \tag{3}$$

where h is the water depth. From (3), (2) becomes

$$\frac{1}{2g}u^2 + h = h_0 \tag{4}$$

Equations (1) and (4) are similar and these equations give the basis of the hydrodynamic analogy of compressible flow.

B. Isentropic Flow

Equation (1) is modified as follows:

$$\frac{h_0}{h} = \frac{T_0}{T} = 1 + \frac{\gamma - 1}{2}M^2 \tag{5}$$

where M is the Mach number, T the static temperature, T_0 the total temperature, and γ the ratio of specific heats. The Mach number is given by

$$M = \frac{u}{a} \tag{6}$$

where $a\left(= \sqrt{\gamma RT}\right)$ is the acoustic velocity and R the gas constant.

Equation (4) becomes

$$\frac{h_0}{h} = 1 + \frac{1}{2}Fr^2 \tag{7}$$

Etsuo Morishita is with Meisei University, 2-1-1 Hodokubo, Hino, Tokyo, 191-8506 Japan (e-mail: etsuo.morishita@ meisei-u.ac.jp).

where Fr is the Froude number, and it is defined as follows:

$$Fr = \frac{u}{c} \tag{8}$$

where $c\left(=\sqrt{gh}\right)$ is the wave velocity of shallow water.

We might regard the shallow water flow as a hypothetical gas flow of $\gamma = 2$. In this case (7) is identical to (5) when $M = Fr$. Although the ratio of specific heats γ is not modeled accurately, (7) becomes the basis of the hydraulic analogy of high-speed flows.

The energy and isentropic relations for gas flows are transformed to those of shallow water flows as:

$$\frac{T_0}{T} = 1 + \frac{\gamma - 1}{2} M^2 \Big|_{\substack{\gamma=2 \\ M=Fr}} = 1 + \frac{1}{2} Fr^2 = \frac{h_0}{h} \tag{9}$$

$$\frac{\rho_0}{\rho} = \left(1 + \frac{\gamma - 1}{2} M^2\right)^{\frac{1}{\gamma-1}} \Big|_{\substack{\gamma=2 \\ M=Fr}} = 1 + \frac{1}{2} Fr^2 = \frac{h_0}{h} \tag{10}$$

$$\frac{p_0}{p} = \left(1 + \frac{\gamma - 1}{2} M^2\right)^{\frac{\gamma}{\gamma-1}} \Big|_{\substack{\gamma=2 \\ M=Fr}} = \left(1 + \frac{1}{2} Fr^2\right)^2 = \left(\frac{h_0}{h}\right)^2 \tag{11}$$

where the right-hand-side h_0 / h represents the ratio of water depth. The temperature and the density ratios of gas flows are given by the depth ratio, and the pressure ratio is given by the square of the depth ratio, respectively, in the shallow water flow.

C. Laval Nozzle

A horizontal open channel flow with a rectangular cross section and a varying width is a hydrodynamic Laval nozzle. Bernoulli's and the continuity equations are

$$\frac{u^2}{2g} + h = h_0 \tag{12}$$

$$Q = uhw \tag{13}$$

where Q is the volumetric flow rate and w the width of the channel. From (12) and (13), we can show

$$\frac{w}{w^*} = \frac{\left[\frac{2}{3}\left(1 + \frac{1}{2} Fr^2\right)\right]^{\frac{3}{2}}}{Fr} \tag{14}$$

The Froude number can be expressed analytically as a function of w / w^* from (14) which differs from gas dynamics [16].

D. Shock Wave and Hydraulic Jump

The pressure ratio across a normal shock wave is

$$\frac{p_2}{p_1} = 1 + \frac{2\gamma}{\gamma + 1}\left(M_1^2 - 1\right) \tag{15}$$

The equivalent equation for a hydraulic jump becomes

$$\frac{P_2}{P_1} = \left(\frac{h_2}{h_1}\right)^2 = \left(\frac{-1 + \sqrt{1 + 8Fr_1^2}}{2}\right)^2 \tag{16}$$

where

$$P \equiv \frac{1}{2} \rho g h^2 \tag{17}$$

is the average force by pressure per unit width of a channel, 1 the shock upstream and 2 the shock downstream.

Fig. 1 shows the ratio of (15) with $\gamma = 1.4, 1.7, 2$, and that of (16). As the upstream Mach number increases, the hydraulic jump pressure ratio becomes higher than that of the hypothetical gas of $\gamma = 2$. So the hydraulic analogy of compressible flows is not necessarily accurate quantitatively where the nonlinear phenomena are dominant.

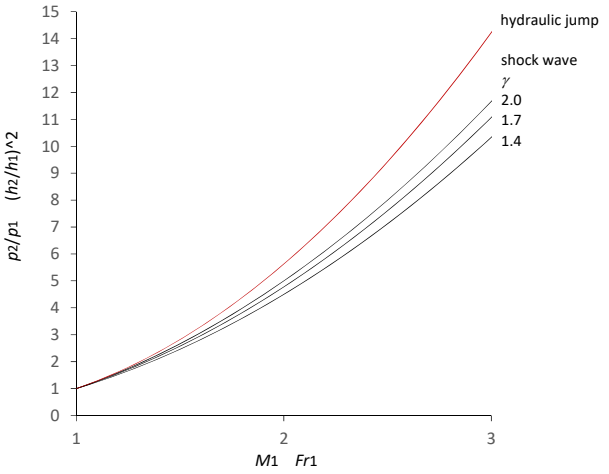

Fig. 1 Normal shock wave and hydraulic jump pressure ratio

The oblique shock conditions for compressible flows become

$$\frac{p_2}{p_1} = 1 + \frac{2\gamma}{\gamma + 1}\left(M_1^2 \sin^2\beta - 1\right) \tag{18}$$

$$\tan\theta = \frac{2\cot\beta\left(M_1^2 \sin^2\beta - 1\right)}{2 + M_1^2\left(\gamma + 1 - 2\sin^2\beta\right)} \tag{19}$$

$$M_2^2 = \frac{\left(\frac{\gamma+1}{2} M_1 \sin\beta\right)^2 M_1^2 - \left(M_1^2 \sin^2\beta - 1\right)\left(\gamma M_1^2 \sin^2\beta + 1\right)}{\left(\gamma M_1^2 \sin^2\beta - \frac{\gamma-1}{2}\right)\left(1 + \frac{\gamma-1}{2} M_1^2 \sin^2\beta\right)} \tag{20}$$

where β is the shock angle and θ the flow deflection angle.

The maximum attached shock angle β_{max} and the sonic shock angle β_* at $M_2 = 1$ become [3]

$$\sin^2\beta_{max} = \frac{(\gamma+1)M_1^2 - 4 + \sqrt{(\gamma+1)\left[(\gamma+1)M_1^4 + 8(\gamma-1)M_1^2 + 16\right]}}{4\gamma M_1^2} \quad (21)$$

$$\sin^2\beta_* = \frac{(\gamma+1)M_1^2 + \gamma - 3 + \sqrt{(\gamma+1)\left[(\gamma+1)M_1^4 + 2(\gamma-3)M_1^2 + (\gamma+9)\right]}}{4\gamma M_1^2} \quad (22)$$

For the hydraulic jump, we can derive equations:

$$\frac{P_2}{P_1} = \left(\frac{h_2}{h_1}\right)^2 = \left(\frac{-1+\sqrt{1+8Fr_1^2\sin^2\beta}}{2}\right)^2 \quad (23)$$

$$\tan\theta = \frac{\left(\sqrt{1+8Fr_1^2\sin^2\beta}-3\right)\tan\beta}{2\tan^2\beta - 1 + \sqrt{1+8Fr_1^2\sin^2\beta}} \quad (24)$$

$$Fr_2^2 = \left[1-\left\{1-\frac{1}{\left(\frac{-1+\sqrt{1+8Fr_1^2\sin^2\beta}}{2}\right)^2}\right\}\sin^2\beta\right]\times\frac{Fr_1^2}{\left(\frac{-1+\sqrt{1+8Fr_1^2\sin^2\beta}}{2}\right)} \quad (25)$$

The sonic condition β_* at $Fr_2 = 1$ for a given Fr_1 is obtained numerically from (25). The sonic wedge angle θ_* is then calculated by (24).

A different form of (24) becomes

$$\theta = \beta - \tan^{-1}\left(\frac{\tan\beta}{\frac{-1+\sqrt{1+8Fr_1^2\sin^2\beta}}{2}}\right) \quad (26)$$

The maximum deflection angle θ_{max} for an attached hydraulic jump is obtained by differentiating (26) by β. The condition becomes

$$\left(-1+\sqrt{1+8Fr_1^2\sin^2\beta}\right)^2\cos^2\beta + 4\sin^2\beta + \frac{16Fr_1^2\sin^2\beta\cos^2\beta}{\sqrt{1+8Fr_1^2\sin^2\beta}} - 2\left(-1+\sqrt{1+8Fr_1^2\sin^2\beta}\right)\Big|_{\theta=\theta_{maax}} = 0 \quad (27)$$

Equation (27) is solved numerically to obtain $\beta = \beta_{max}$ and we can determine θ_{max} from (24) and/or (26).

Fig. 2 shows the oblique shock wave and hydraulic jump relationship. For air, we get $M_2 : \theta : \beta\big|_* = 1 : 22.7^\circ : 61.5^\circ$; $M_2 : \theta : \beta\big|_{max} = 0.924 : 23.0^\circ : 64.7^\circ$ at $M = 2$. For water, we get $Fr_2 : \theta : \beta\big|_* = 1 : 18.4^\circ : 57.2^\circ$; $Fr_2 : \theta : \beta\big|_{max} = 0.84 : 19.6^\circ : 64.5^\circ$ at $Fr = 2$. The oblique hydraulic jump is similar to an oblique shock wave of $\gamma = 1.7$, although the flow deflection angles θ_* at the sonic condition are different.

Fig. 3 shows (24) with θ_* from $Fr_2 = 1$ in (25) and θ_{max} from (27).

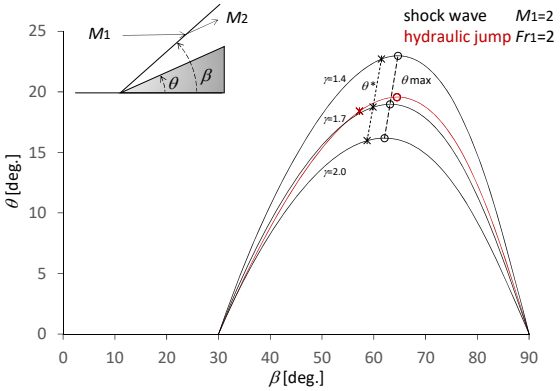

Fig. 2 Oblique shock wave and hydraulic jump at $M = Fr = 2$

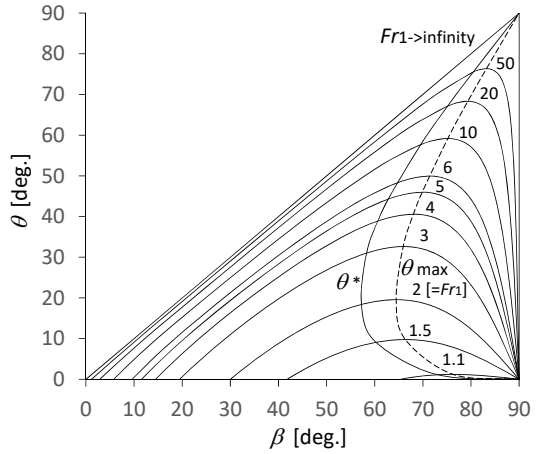

Fig. 3 Oblique hydraulic jump

We get

$$\beta = \theta \quad (28)$$

when the upstream Froude number Fr_1 increases toward infinity in in (26).

The velocity components in the *x*- and *y*-directions behind the oblique shock wave become:

$$V_{2x} \equiv V_2\cos\theta = V_1\cos^2\beta + \frac{V_1\sin^2\beta}{\left(\frac{h_2}{h_1}\right)} \quad (29)$$

$$V_{2y} \equiv V_2 \sin\theta = \frac{V_1 - V_{2x}}{\tan\beta} \tag{30}$$

where V_1 is the uniform flow velocity and V_2 the velocity behind the shock wave. We can derive the shock polar equation from (23), (29) and (30) by eliminating the angle β as follows

$$x = b\frac{y^2}{(b-x)^2 + y^2} + \frac{2b\dfrac{(b-x)^2}{(b-x)^2 + y^2}}{\sqrt{1 + 8Fr_1^2 \dfrac{(b-x)^2}{(b-x)^2 + y^2}} - 1} \tag{31}$$

where we define the symbols for brevity in (31) as:

$$b \equiv \frac{V_1}{c_1^*} = Fr_1^* \tag{32}$$

$$(x, y) \equiv \frac{1}{c_1^*}(V_{2x}, V_{2y}) \tag{33}$$

The characteristic Froude number is defined as

$$Fr_1^{*2} \equiv \left(\frac{V_1}{c_1^*}\right)^2 = \frac{3Fr_1^2}{2 + Fr_1^2} \tag{34}$$

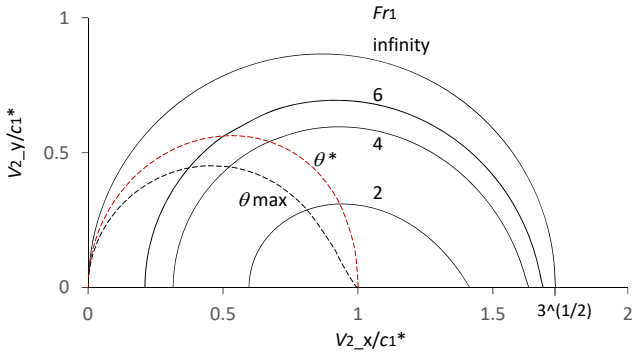

Fig. 4 Shock polar for hydraulic jump

We can draw the shock polar either from (29) and (30) by changing β or (31) as shown in Fig. 4. When we increase the upstream Mach number toward infinity

$$Fr_1^*\big|_{Fr_1 \to \infty} = \sqrt{3}$$

Therefore, we can show from (31) that the shock polar in this case becomes a circle which passes the origin that is different from gas dynamics:

$$\left(\frac{V_{2x}}{c_1^*} - \frac{\sqrt{3}}{2}\right)^2 + \left(\frac{V_{2y}}{c_1^*}\right)^2 = \left(\frac{\sqrt{3}}{2}\right)^2 \tag{35}$$

The locus of the maximum flow deflection $\theta_{\max}$ from (27) and the sonic condition θ^* from $Fr_2 = 1$ from (25) are also shown in Fig. 4. From the definition, we get

$$Fr_2^2 = \frac{V_2^2}{gh_2^2} = \frac{V_2^2}{gh_1^*}\frac{h_1^*}{h_1}\frac{h_1}{h_2}$$
$$= (x^2 + y^2)\left[\frac{2}{3}\left(1 + \frac{1}{2}Fr_1^2\right)\right]\frac{1}{\left[\dfrac{-1 + \sqrt{1 + 8Fr_1^2\dfrac{(b-x)^2}{(b-x)^2 + y^2}}}{2}\right]} \tag{36}$$

We can also determine the locus of the sonic condition θ^* as a cross point of (31) and (36) =1 in Fig. 4.

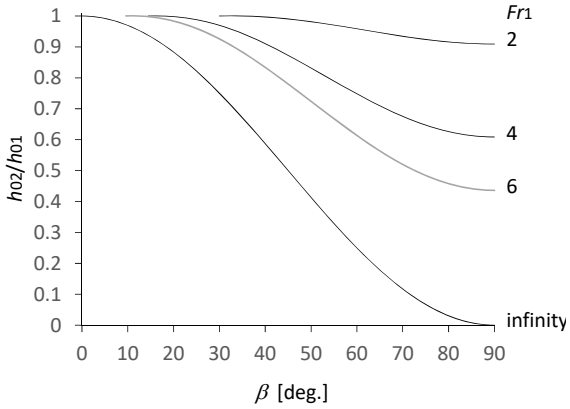

Fig. 5 Total head loss through an oblique hydraulic jump

The critical velocity changes as is the case for the total head through a hydraulic jump in (37) and Fig. 5 while it is constant in gas dynamics because the total enthalpy is conserved.

$$\frac{h_{02}}{h_{01}} = \frac{h_2^*}{h_1^*} = \frac{c_{2*}^2}{c_{1*}^2} = 1 - \frac{1}{4}\frac{\left(\dfrac{h_2}{h_1} - 1\right)^3}{\left(\dfrac{h_2}{h_1}\right)}\frac{1}{\left(\dfrac{h_{01}}{h_1}\right)}$$
$$= 1 - \frac{1}{4}\frac{\left(\dfrac{-1 + \sqrt{1 + 8Fr_1^2 \sin^2\beta}}{2} - 1\right)^3}{\left(\dfrac{-1 + \sqrt{1 + 8Fr_1^2 \sin^2\beta}}{2}\right)}\frac{1}{1 + \dfrac{1}{2}Fr_1^2} \tag{37}$$

The total energy is actually conserved also in hydraulics as:

$$\frac{u^2}{2g} + h + \frac{CT}{g} = h_0 \tag{38}$$

where C is the specific heat of water and T the static

temperature. However, the temperature difference across the hydraulic jump of $\Delta h_0 = h_{01} - h_{02} = 1\text{m}$ in water is negligible due to the heat capacity of water as is expected:

$$\Delta T = \frac{g}{C}\Delta h_0\Big|_{\Delta h_0=1m} \approx \frac{9.8\times 1}{4200} << 1$$

E. Prandtl-Meyer Expansion

The continuity and the momentum equations for a two-dimensional steady flow become [2]

$$hu\Delta n = \text{const.} \tag{39}$$

$$hu\frac{\partial u}{\partial s} = -\frac{1}{\rho}\frac{\partial P}{\partial s} \tag{40}$$

where Δn is the streamline width, s the streamline coordinate. We can derive the following equation from (39) and (40):

$$\cot^2\mu\frac{1}{u}\frac{\partial u}{\partial s} - \frac{\partial \theta}{\partial n} = 0 \tag{41}$$

where θ is the flow direction. The irrotational condition is given by

$$\frac{\partial u}{\partial n} - u\frac{\partial \theta}{\partial s} = 0 \tag{42}$$

We introduce the Prandtl-Meyer angle ν as:

$$d\nu \equiv \cot\mu\frac{du}{u} \tag{43}$$

Equations (41) and (42) become

$$\frac{\partial \nu}{\partial s} - \tan\mu\frac{\partial \theta}{\partial n} = 0 \tag{44}$$

$$\tan\mu\frac{\partial \nu}{\partial n} - \frac{\partial \theta}{\partial s} = 0 \tag{45}$$

The sum and the difference of (44) and (45) become

$$\frac{\partial}{\partial s}(\nu - \theta) + \tan\mu\frac{\partial}{\partial n}(\nu - \theta) = 0 \tag{46}$$

$$\frac{\partial}{\partial s}(\nu + \theta) - \tan\mu\frac{\partial}{\partial n}(\nu + \theta) = 0 \tag{47}$$

We have the Riemann invariant as:

$$\nu - \theta = R \quad : C^+ \tag{48}$$

$$\nu + \theta = Q \quad : C^- \tag{49}$$

The following relationships are derived from the definition:

$$d\nu = \cot\mu\frac{du}{u} = \frac{\cos\mu}{\sin\mu}\frac{du}{u} = \frac{\sqrt{1-\left(\frac{c}{u}\right)^2}}{\left(\frac{c}{u}\right)}\frac{du}{u} = \sqrt{Fr^2-1}\frac{du}{u}$$

$$u = Frc$$

$$\frac{du}{u} = \frac{dFr}{Fr} + \frac{dc}{c}$$

$$c = \frac{c_0}{\left(1+\frac{1}{2}Fr^2\right)^{\frac{1}{2}}}$$

$$\frac{dc}{c} = -\frac{1}{2}\frac{Fr}{1+\frac{1}{2}Fr^2}dFr$$

Thus we have

$$d\nu = \frac{1}{2}\frac{\sqrt{Fr^2-1}}{1+\frac{1}{2}Fr^2}\frac{dFr^2}{Fr^2} \tag{50}$$

$$\nu(Fr) = \sqrt{3}\tan^{-1}\sqrt{\frac{Fr^2-1}{3}} - \tan^{-1}\sqrt{Fr^2-1} \tag{51}$$

Equations (50) and (51) are the same as those of a hypothetical gas of γ=2.

F. Linearized Supersonic Flow

The continuity and the momentum equations in hydraulics are

$$\frac{\partial h}{\partial t} + \nabla\cdot h\mathbf{v} = 0 \tag{52}$$

$$\frac{\partial h\mathbf{v}}{\partial t} + \nabla\cdot(h\mathbf{v}\mathbf{v}) + \frac{1}{\rho}\nabla P = 0 \tag{53}$$

where $\mathbf{v} = (u,v)$ is the velocity vector in the $x-y$ coordinate.. We introduce the two-dimensional velocity potential ϕ as:

$$\mathbf{v} = \nabla\phi \tag{54}$$

The steady continuity equation becomes

$$\nabla\cdot h\mathbf{v} = \frac{\partial hu}{\partial x} + \frac{\partial hv}{\partial y} = h(\phi_{xx} + \phi_{yy}) + \phi_x\frac{\partial h}{\partial x} + \phi_y\frac{\partial h}{\partial y} = 0 \tag{55}$$

The steady momentum equation is obtained from (53) with (52) as:

$$\mathbf{v}\cdot\nabla\mathbf{v} + \frac{1}{\rho h}\nabla P = 0 \tag{56}$$

$$VdV = -gdh \tag{57}$$

where $V = |\mathbf{v}| = \sqrt{u^2 + v^2}$. From (57)

$$dh = -\frac{1}{2}\frac{h}{c^2}d\left(\phi_x^2 + \phi_y^2\right) \tag{58}$$

$$\frac{\partial h}{\partial x} = -\frac{1}{2}\frac{h}{c^2}\frac{\partial}{\partial x}\left(\phi_x^2 + \phi_y^2\right) = -\frac{h}{c^2}\left(\phi_x\phi_{xx} + \phi_y\phi_{yx}\right) \tag{59}$$

$$\frac{\partial h}{\partial y} = -\frac{1}{2}\frac{h}{c^2}\frac{\partial}{\partial y}\left(\phi_x^2 + \phi_y^2\right) = -\frac{h}{c^2}\left(\phi_x\phi_{xy} + \phi_y\phi_{yy}\right) \tag{60}$$

From (55), (59) and (60), we have the full potential equation which is exactly the same as that of gas dynamics [9].

$$\left(c^2 - \phi_x^2\right)\phi_{xx} - 2\phi_x\phi_y\phi_{xy} + \left(c^2 - \phi_y^2\right)\phi_{yy} = 0 \tag{61}$$

The linearized form of (61) becomes

$$\left(Fr_\infty^2 - 1\right)\phi_{xx} - \phi_{yy} = 0 \tag{62}$$

From the pressure coefficient C_p for $\gamma = 2$ and $M_\infty = Fr_\infty$ [11], we get with (11)

$$C_p \equiv \frac{p - p_\infty}{\frac{1}{2}\rho u_\infty^2} = \frac{2}{\gamma M_\infty^2}\left(\frac{p}{p_\infty} - 1\right) = \frac{1}{Fr_\infty^2}\left[\left(\frac{h}{h_\infty}\right)^2 - 1\right] \tag{63}$$

where u_∞ is the uniform velocity Equation (63) may be redefined with (17) in the hydraulics style as

$$C_p \equiv \frac{P - P_\infty}{\frac{1}{2}\rho u_\infty^2 \cdot h_\infty^2} = \frac{1}{Fr_\infty^2}\left[\left(\frac{h}{h_\infty}\right)^2 - 1\right] \tag{64}$$

For the small disturbances denoted by dash,

$$h = h_\infty + h'$$

$$u = u_\infty + u'$$

$$v = v'$$

$$\frac{\left(u_\infty + u'\right)^2 + v'^2}{2g} + \left(h_\infty + h'\right) = h_0$$

We neglect the higher terms and

$$\frac{u_\infty^2}{gh_\infty}\frac{u'}{u_\infty} + \frac{h'}{h_\infty} = 0$$

Thus we have

$$C_p = \frac{1}{Fr_\infty^2}\left[\left(\frac{h_\infty + h'}{h_\infty}\right)^2 - 1\right] \approx -\frac{2u'}{u_\infty} \tag{65}$$

Equation (62) may have a solution as:

$$\phi = u_\infty f\left(x - \beta y\right) \tag{66}$$

where ϕ is the disturbance potential [2] and

$$\beta = \sqrt{Fr^2 - 1} \tag{67}$$

The boundary condition on the body surface becomes

$$\frac{dy}{dx}\left(\approx \theta\right) = \frac{v'}{u_\infty + u'} \approx \frac{v'}{u_\infty} = \frac{\phi_y}{u_\infty} = -\beta \cdot f' \tag{68}$$

Equation (65) with (68) becomes

$$C_p = -2\frac{u'}{u_\infty} = -2\frac{\phi_x}{u_\infty} = -2f' = \frac{2\theta}{\beta} = \frac{2\theta}{\sqrt{Fr^2 - 1}} \tag{69}$$

Equation (69) gives the same formula as that of gas dynamics.

G. Hydraulic Fanno Flow

A horizontal open channel flow in a rectangular cross section with friction is an equivalent to Fanno flow in gas dynamics. We assume that the width of the channel is infinite and the flow is two-dimensional. The continuity and the momentum equations become

$$\frac{\partial h}{\partial t} + \frac{\partial hu}{\partial x} = 0 \tag{70}$$

$$\frac{\partial}{\partial t}hu = -\frac{\partial}{\partial x}\left[hu\right]u - \frac{1}{\rho}\frac{\partial P}{\partial x} - \frac{\tau}{\rho} \tag{71}$$

where t is the time, τ the friction, and

$$\tau \equiv \frac{1}{2}\rho u^2 C_f \tag{72}$$

where C_f is the average friction coefficient along the flow passage and it is therefore a constant. For a steady flow, (70) and (71) become

$$q \equiv uh = u^* h^* \left(= \text{const.}\right) \tag{73}$$

$$udu + gdh + \frac{1}{h}\frac{C_f}{2}u^2 dx = 0 \tag{74}$$

where q is the volumetric flow rate per unit width. From (73)

and (74),

$$C_f \frac{dx}{h^*} = \frac{4}{3}\left(\frac{1}{Fr^{\frac{11}{3}}} - \frac{1}{Fr^{\frac{5}{3}}}\right)dFr \tag{75}$$

We can integrate (75) as:

$$\frac{C_f}{h^*}\int_x^{x^*} dx = \frac{4}{3}\int_{Fr}^{1}\left(\frac{1}{Fr^{\frac{11}{3}}} - \frac{1}{Fr^{\frac{5}{3}}}\right)dFr \tag{76}$$

Finally we get the following equation [17].

$$4C_f \frac{L^*}{h^*} = 6 - \frac{8}{Fr^{\frac{2}{3}}} + \frac{2}{Fr^{\frac{8}{3}}} \tag{77}$$

$$4C_f \frac{L^*}{h^*} = 6 - 8\left(\frac{h}{h^*}\right) + 2\left(\frac{h}{h^*}\right)^4 \tag{78}$$

where

$$L^* \equiv x^* - x \tag{79}$$

The factor four comes from the definition of the pipe friction coefficient λ

$$\lambda = 4C_f \tag{80}$$

In hydraulics, Manning's formula becomes

$$u^2 = \frac{1}{n^2} h^{\frac{4}{3}} i \tag{81}$$

where i is the channel gradient, n the roughness factor and the width of a rectangular channel is assumed to be infinite. For a horizontal rectangular channel of infinite width, we may put hydraulically

$$\Delta p = \rho g \Delta h = \lambda \frac{l}{4h} \cdot \frac{1}{2}\rho u^2 \tag{82}$$

where l is the channel length, Δp the pressure loss, Δh the head loss, and $4h$ the hydraulic diameter. From (81) and (82), we may equate the channel gradient i to the head gradient as:

$$i = \frac{\Delta h}{l} = \frac{n^2}{h^{\frac{4}{3}}} u^2 = \lambda \frac{1}{g(4h)} \frac{1}{2} u^2$$

Thus we get

$$\lambda = \frac{8gn^2}{h^{\frac{1}{3}}} \tag{83}$$

From (83) with (80), we have the friction coefficient C_f as a function of the water depth h.

$$C_f = \frac{2gn^2}{h^{\frac{1}{3}}} = \frac{\frac{2gn^2}{h^{*\frac{1}{3}}}}{\left(\frac{h}{h^*}\right)^{\frac{1}{3}}} = \frac{C_{f\,\text{Manning}}}{\left(\frac{h}{h^*}\right)^{\frac{1}{3}}} \tag{84}$$

$$C_{f\,\text{Manning}} \equiv \frac{2gn^2}{h^{*\frac{1}{3}}} \ (\text{const.}) \tag{85}$$

We have for the Manning's case [18], [19]

$$4C_{f\,\text{Manning}} \frac{L^*}{h^*} = \frac{54}{13} - \frac{6}{Fr^{\frac{8}{9}}} + \frac{\left(\frac{24}{13}\right)}{Fr^{\frac{26}{9}}} \tag{86}$$

$$4C_{f\,\text{Manning}} \frac{L^*}{h^*} = \frac{54}{13} - 6\left(\frac{h}{h^*}\right)^{\frac{4}{3}} + \frac{24}{13}\left(\frac{h}{h^*}\right)^{\frac{13}{3}} \tag{87}$$

When the Froude number goes to infinity, we get

$$\left(\frac{h}{h^*}\right)_{Fr\to\infty} = 0$$

$$4C_f \frac{L^*}{h^*}\Big|_{Fr\to\infty} = 6$$

$$4C_{f\,\text{Manning}} \frac{L^*}{h^*}\Big|_{Fr\to\infty} = \frac{54}{13}$$

For Fanno flow, we have [3]

$$4C_f \frac{L^*}{d} = \frac{1}{\gamma}\frac{1-M^2}{M^2} + \frac{\gamma+1}{2\gamma}\ln\frac{\frac{\gamma+1}{2}M^2}{1+\frac{\gamma-1}{2}M^2} \tag{88}$$

$$\frac{\rho}{\rho^*} = \sqrt{\frac{1+\frac{\gamma-1}{2}M^2}{\frac{\gamma+1}{2}M^2}} \tag{89}$$

The density ratio ρ/ρ^* is equivalent to the depth ratio h/h^*. When the Mach number approaches to infinity, we have

$$4C_f \frac{L^*}{d}\Big|_{M\to\infty} = -\frac{1}{\gamma} + \frac{\gamma+1}{2\gamma}\ln\frac{\gamma+1}{\gamma-1}$$

$$\frac{\rho}{\rho^*}\Big|_{M\to\infty} = \sqrt{\frac{\gamma-1}{\gamma+1}}$$

The density ratio of gas remains finite for M infinity while the depth ratio of water goes to zero for Fr infinity, see Fig. 6.

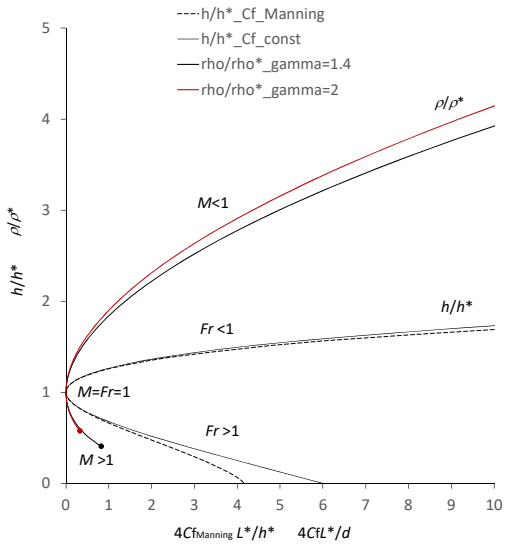

Fig. 6 Fanno flow ρ/ρ^* and horizontal open channel flow h/h^*

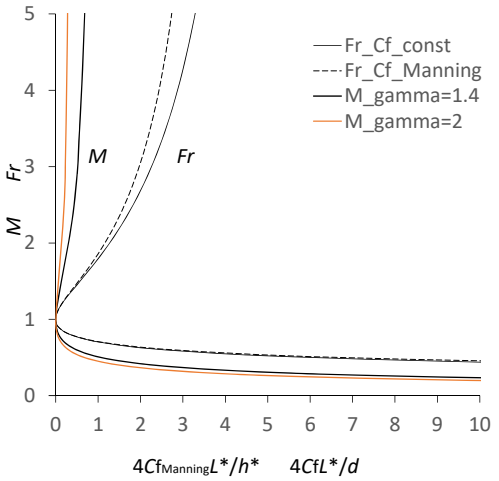

Fig. 7 Fanno flow M and horizontal open channel flow Fr

Equations (77), (78), and (86)-(89) are shown in Figs. 6 and 7. From Figs. 6 and 7, the similarity is clearly visible between Fanno flow and the horizontal open channel flow with friction, although the values are very different. The choke condition is reached only at the exit both in hydraulics and gas dynamics. Both the sub- and the super-critical flows change the Mach number as well as the Froude number toward the sonic and/or critical condition. Total head decreases downstream while entropy increases. In hydraulics, however, the term entropy is less common. This could be due to the fact that loss is negligible to the heat capacity of water [11].

H. Shock Tube Analogy by Hydraulics

The shock tube experiment in gas dynamics might be simulated by the hydrodynamic shock tube, i.e., the dam-break problem of water depth h_1 and h_4 as shown in Fig. 8.

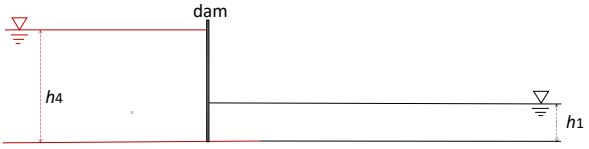

Fig. 8 Hydrodynamic shock tube initial condition

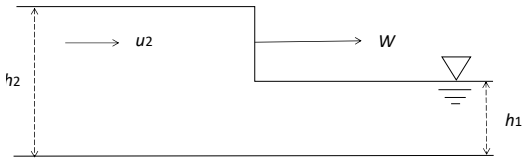

Fig. 9 Moving hydraulic jump

Fig. 9 shows the moving hydraulic jump where h_1 is the stationary water depth, h_2 the moving water depth, u_2 the flow velocity, and W the hydraulic jump wave velocity.

The continuity and the momentum equations in the moving frame of reference become

$$\rho h_1 W = \rho h_2 (W - u_2) \tag{90}$$

$$(\rho h_1 W) W + \frac{1}{2}\rho g h_1^2 = [\rho h_2 (W - u_2)](W - u_2) + \frac{1}{2}\rho g h_2^2 \tag{91}$$

From (90) and (91)

$$W = \sqrt{g h_1}\sqrt{\frac{1}{2}\frac{h_2}{h_1}\left(\frac{h_2}{h_1}+1\right)} \tag{92}$$

$$Fr_1 \equiv \frac{W}{c_1} = \sqrt{\frac{1}{2}\frac{h_2}{h_1}\left(\frac{h_2}{h_1}+1\right)} \tag{93}$$

where

$$c_1 = \sqrt{g h_1} \tag{94}$$

We get h_2/h_1 from (93) and the same solution is obtained as (16). From (90):

$$u_2 = \sqrt{g h_1}\sqrt{\frac{1}{2}\frac{h_2}{h_1}\left(\frac{h_2}{h_1}+1\right)}\left[1 - \frac{1}{\left(\frac{h_2}{h_1}\right)}\right] \tag{95}$$

$$Fr_2 = \frac{u_2}{\sqrt{g h_2}} = \sqrt{\frac{1}{2}\left(\frac{h_2}{h_1}+1\right)}\left[1 - \frac{1}{\left(\frac{h_2}{h_1}\right)}\right] \tag{96}$$

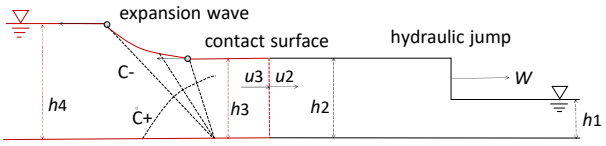

Fig. 10 Hydraulic jump and expansion after dam break

Along the characteristics C^+ from the stationary region 4 in Fig. 10, the Riemann invariant P becomes [2]

$$P = u + 2c = 2c_4 \tag{97}$$

and we get from (97)

$$\frac{c}{c_4} = 1 - \frac{1}{2}\left(\frac{u}{c_4}\right) \tag{98}$$

$$\frac{h}{h_4} = \left[1 - \frac{1}{2}\left(\frac{u}{c_4}\right)\right]^2 \tag{99}$$

Along the expansion characteristics C^-, we have

$$\frac{dx}{dt} = u - c \tag{100}$$

where t is the time, and x the coordinate. The characteristics C^+ form the stationary region 4 have the same values of the Riemann invariant P in (97), and cross the each characteristics C^- with the Riemann invariant $Q = u - 2c$. This means that u and c are constant along the same characteristic line C^- [9], and we get

$$x = (u - c)t \tag{101}$$

From (98) and (101),

$$u = \frac{2}{3}\left(c_4 + \frac{x}{t}\right) \qquad -c_4 t \le x \le (u_3 - c_3)t \tag{102}$$

From (99) and $u_2 = u_3$, we have

$$\frac{h_3}{h_4} = \left[1 - \frac{1}{2}\left(\frac{u_3}{c_4}\right)\right]^2 = \left[1 - \frac{1}{2}\left(\frac{u_2}{c_4}\right)\right]^2 = \frac{h_2}{h_4} \tag{103}$$

$$u_2 = u_3 = 2c_4\left[1 - \left(\frac{h_2}{h_4}\right)^{\frac{1}{2}}\right] \tag{104}$$

From (95) and (104), we can derive

$$\frac{h_4}{h_1} = \frac{h_2}{h_1}\left[1 + \frac{1}{2}\sqrt{\frac{1}{2}\left(\frac{h_2}{h_1} + 1\right)}\left(1 - \frac{1}{\left(\frac{h_2}{h_1}\right)}\right)\right]^2 \tag{105}$$

From (105), h_2/h_1 is obtained for a given h_4/h_1. The hydrodynamic shock tube, i.e., the dam-break problem solution is shown in Fig. 11.

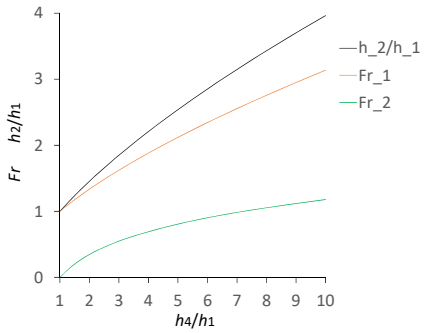

Fig. 11 Hydrodynamic shock tube solution

III. High-Speed Flow Analogue in a Tin Box

A. Under Expanded Nozzle in a Shallow Water

We frequently observe the high-speed analogies of shallow water supercritical flow.

Fig. 12 shows a circular hydraulic jump in a tin box cover. Many engineering students are rather awed when they learn that this circle is an equivalent of a shock wave of supersonic flow.

Fig. 13 is a flow from an extensible tap in Fig. 12 touched on a tin box cover. The surrounding water depth is about 4 mm. This flow is similar to that of an under expanded nozzle. The jet free boundary is formed by the circumferential water head. First, a water flow from the tap expands to the super-critical condition and then turns by the surrounding head, i.e. the ambient pressure by forming the barrel shock, and then forms a first pair of oblique shock waves. The flows on the both sides of the center line turn inward and develop the second pair of oblique shock wave and a character x-like pattern is formed.

When the flow rate is decreased from the condition in Fig. 13 and/or the downstream head is increased, a Mach disc appears as in Fig. 14.

In gas dynamics, we need a supersonic wind tunnel to test these phenomena and the experiment requires very expensive measurement equipment. In a tin box experiment, however, we can visualize the nozzle exit flow easily and understand the flow physics precisely. It is therefore very valuable for engineering education in general.

There are explanations on the nozzle exit flow in the text book of gas dynamics [7], and most simply one can describe the flow in Fig. 13 by the one expansion wave from the nozzle exit with one reflected shock from the constant pressure boundary. The Mach disc in Fig. 14 is also explained by Saad [7] as "downstream of this pattern, the flow is rotational and consists

of subsonic and supersonic regions."

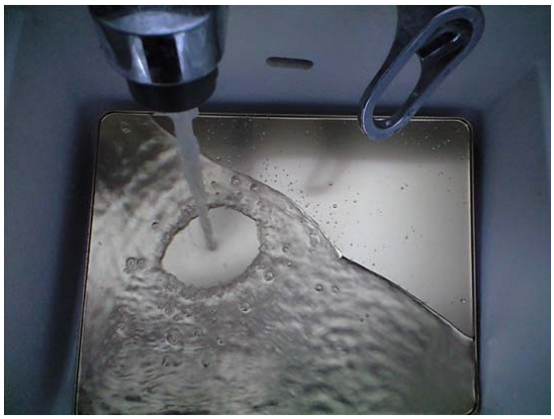

Fig. 12 Hydraulic jump in a tin box cover

Fig. 13 Under expanded nozzle flow in a shallow water

Fig. 14 Mach disc in a shallow water

B. Diamond Airfoil

Fig. 15 shows a diamond airfoil of $\tau/c=1/3$ moving manually with a bar in a tin box with 5 mm water depth where c is the chord and τ the thickness. The semi apex angle θ is about 16.9 degrees. From two movie shots with time lapse 0.1 second, the Froude number is approximately $Fr \approx 2.3$ ($M \approx 2.3$). The oblique shock wave angle form the leading edge in Fig. 15 appears about $\beta \approx 45^{\circ}$. This result coincides with that shown in Fig. 3. Although this experiment requires only a tin box and a model diamond airfoil, we can physically observe the oblique shock waves form the leading and the trailing edges. The Prandtl-Mayer expansion wave is also visible form the two apexes although it is not quite clear.

We apply the shock-expansion method to the experiment in Fig. 15 and obtain the result shown in Fig. 16 where the interaction between the shocks and the expansion fans is simplified.

We assume that the two characteristic lines C^+ form the apex interact with the front and rear shock waves once, respectively, while continuous interactions take place physically. The first characteristic line C^+ represents the flow turned five degrees from the initial expansion, and the second characteristic line C^+ is the flow turning another five degrees to the end of the expansion. The shock waves are weakened by the expansion fans and the inclination of the shock waves approach to that of the Mach wave. The front shock wave decreases the inclination to the downstream while the second one increases the wave angle by the interaction.

We can estimate the water depth ratio h/h_1, the Froude number Fr and the pressure coefficient Cp as shown in Figs. 17-19 from the shock expansion method. The linearized pressure coefficient is also shown in Fig. 19. While the expansion is relatively well predicted by the linear theory, the shock side is underestimated by the linear theory. This is due to the apex angle of the diamond airfoil.

The surface tension wave is also observed and this is very different from gad dynamics. So the hydrodynamic analogy has its own limitation as known from many decades ago [5].

Hatch conducted detailed measurements of diamond and circular arc airfoils of both 6% thickness by hydraulic analogy [11]. The diamond airfoil is shown in Fig. 20 and the maximum thickness locates at 30% chord.

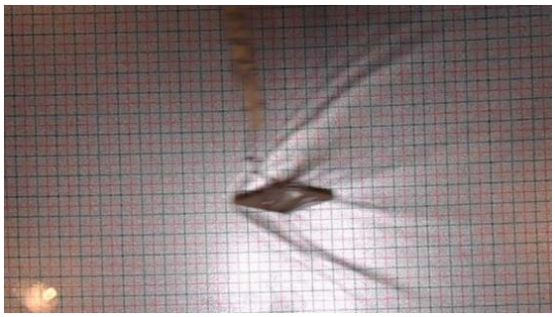

Fig. 15 Diamond airfoil in a tin box of 5mm water depth $Fr(M) \approx 2.3$ (Photo by D. Yamagishi)

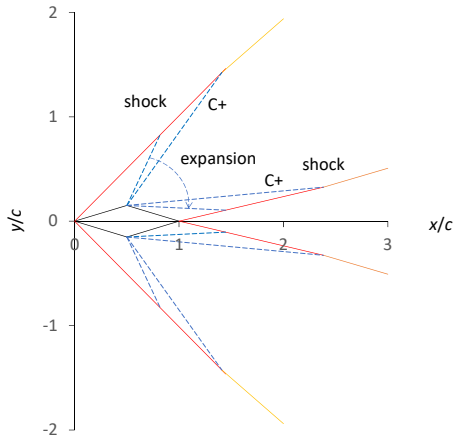

Fig. 16 Diamond airfoil by shock-expansion method $Fr(M)=2.3$

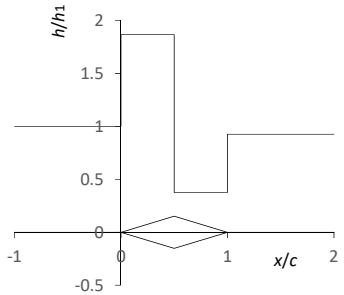

Fig. 17 Water depth ratio h/h_1 by shock-expansion method $Fr=2.3$

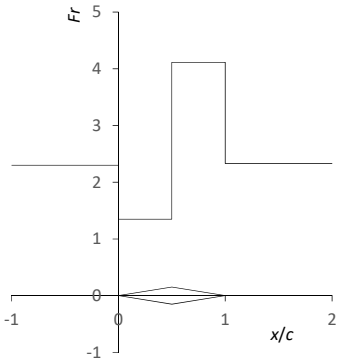

Fig. 18 Froude number Fr by shock-expansion method $Fr=2.3$

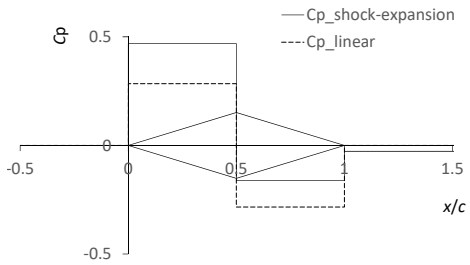

Fig. 19 Pressure coefficient C_p $Fr=2.3$

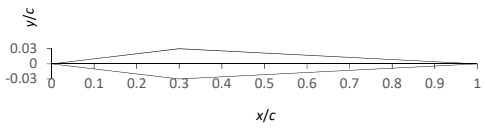

Fig. 20 Diamond airfoil [11]

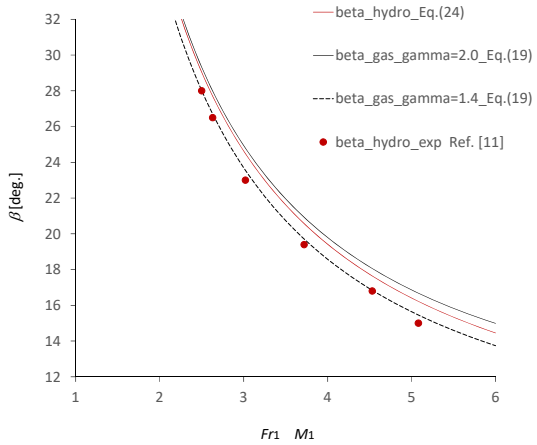

Fig. 21 Diamond airfoil shock wave inclined angle β

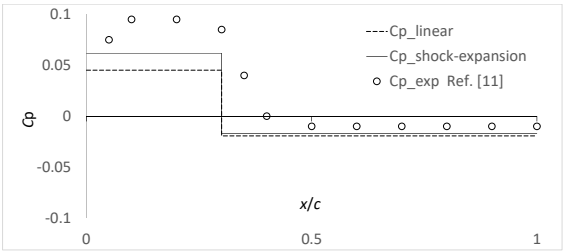

Fig. 22 Surface pressure coefficient of diamond airfoil $Fr_1=4.53$

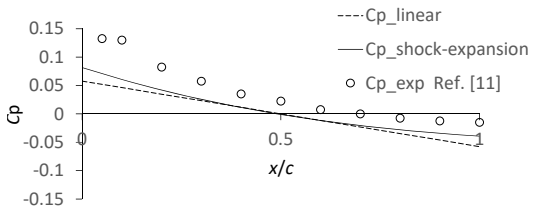

Fig. 23 Surface pressure coefficient of 6 % circular arc airfoil $Fr_1=4.26$

Hatch measured the shock angles from the photos as shown in Fig. 21 where the theoretical formulas are also shown for water and gas. The experimental results ostensibly agree with the formula for air $\gamma=1.4$ while the theoretical β for water by (24) is slightly higher than that of experiment. The theory, however, well predicts the physical aspect of the oblique hydraulic jump.

Fig. 22 shows the pressure coefficient obtained by Hatch [11] which is higher than that of the ideal theoretical predictions although the expansion side shows better results.

The linear and the shock-expansion theories are applied to a

circular arc airfoil in a supersonic flow. The hydraulic experiment by Hatch [11] is shown in Fig. 23. The experimental results are larger than those of the theoretical ones, and this is possibly due to the viscous effect.

C. Circular Cylinder

Figs. 24 (a) and (b) show a detached shock wave (hydraulic jump) around a moving circular cylinder in a tin box of 5 mm water depth in 0.2 seconds. We can estimate the approximate shock stand-off distance from the picture.

The empirical formula for the shock stand-off distance for a circular cylinder in supersonic air flow [20] is shown in Fig. 25. The present experiments ostensibly agree with the formula for air flow, but care must be taken that the hypothetical specific ratio γ=2 is different from that of air, and the present experiment is not intended for a precise measurement. Fig. 25 gives higher value than that of experiments for air [2], [21].

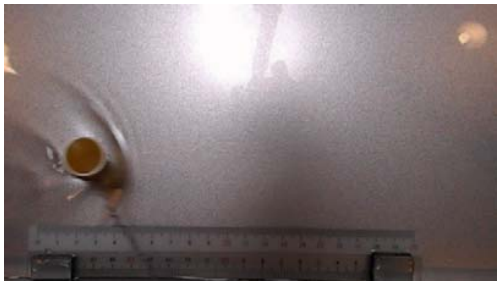

(a) t = 0 [s]

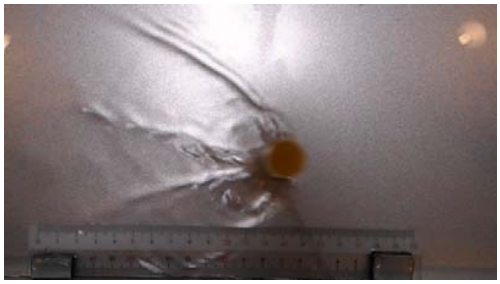

(b) t = 0.2 [s]

Fig. 24 Detached shock wave around a moving circular cylinder in a tin box of 5mm water depth $Fr(M) \approx 2.4$ (Photo by D. Yamagishi)

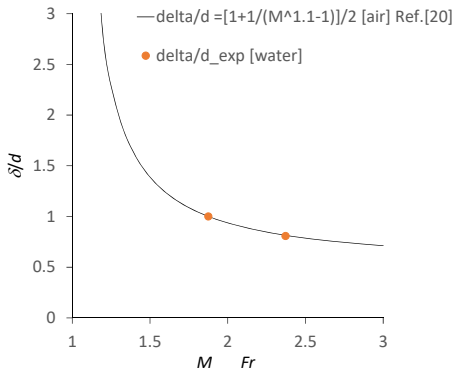

Fig. 25 Shock stand-off distance

D. Riemann Problem

A shock tube analysis is called the Riemann problem in gas dynamics. The equivalent phenomenon is a dam break in hydraulics.

We can conduct a desktop dam breaking experiment by a plastic box. A semi-transparent plastic box of about 270 mm bottom length x 75 mm depth x 80 mm bottom width is prepared. The cross section is trapezoidal with 90 mm opening. The box is filled with shallow water, and a balsa gate covered by a cloth seal is inserted to produce a water level difference as shown Fig. 26 (t=0) where the high side depth is about 12 mm and the lower side depth is about 6 mm, respectively. Water in the left hand side is colored by drips of soy source. We also tested tea in the past experiment [15]. The gate is quickly moved upward manually and the dam breaking phenomena is recorded as a movie of which several scenes are shown in Figs. 26 (a')-(d').

The eperiment is compared to the analytical solution of the Riemann problem and the numerical method of characteristics in Figs. 26 (a)-(d). In the analytical solution, the reflected hydraullic jump from the rght wall is considered while the reflection of expansin wave from the left wall is not included which the numericall method of characteristics incorporates automatically.

Just after the gate is open, the right-running hydraulic jump and the left-running expansion wave are formed, respectively. The contact surface is clearly visible in this experiment which is very difficult to visualize in the gas experiment. The moving hydraulic jump is not clear but we can see it as a movie.

Because the left wall is closer, the expansion wave reaches to the wall first as (c) and (c') in Fig. 26. Analytical, numerical and experimental results are not necessarily identical for the arrival time, but the same physics are observed.

The hydraulic jump reaches to the right wall as in (d) and (d') of Fig. 26, and reflected to the contact surface as (e) and (e') in Fig. 26. In theory, the contact surface stands still after the reflected shock wave passes. In reality the contact surface is not stationary possibly due to the reflected expansion wave from the left hand side.

This desktop dam break experiment is a very good tool to study the real shock tube although it does not necessarily give the accuracy of the measurement. Students see the shock wave, the expansion wave and even the colored contact surface and reach the quick understanding of the Riemann problem.

IV. Conclusion

The shallow water analogy of high-speed aerodynamics is revisited and several experiments are proposed for engineering students. The theoretical analogical comparisons are described for the isentropic flow, the normal shock and oblique waves, the Prandtl-Meyer expansion, the full potential equation, the linearized supersonic flow, and the method of characteristics. The under expanded nozzle and the Mach disc are observed easily and the supersonic external flows around a circular cylinder and a diamond airfoil are tested in a shallow tin box. A desktop Riemann problem is also introduced, and it is

interesting to note that the contact surface is easily visualized for engineering students' comprehension.

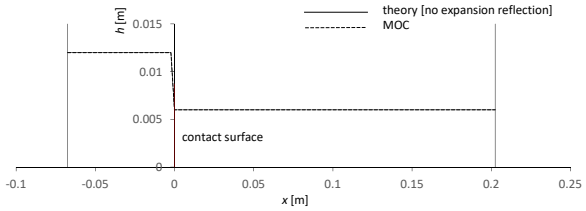

(a) t =0 [s]

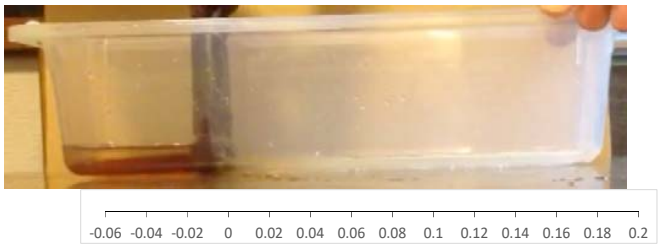

(a') time 00:94 t=0 [s]

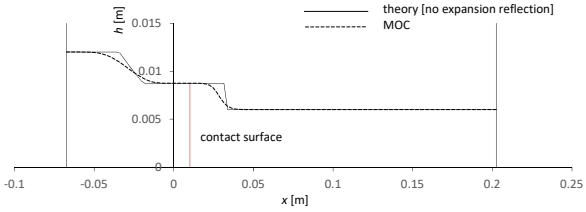

(b) t=0.1 [s]

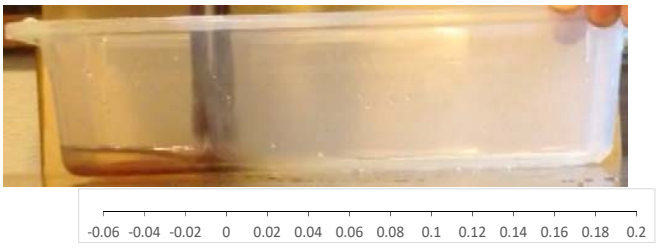

(b') time 01:04 t=0.1 [s]

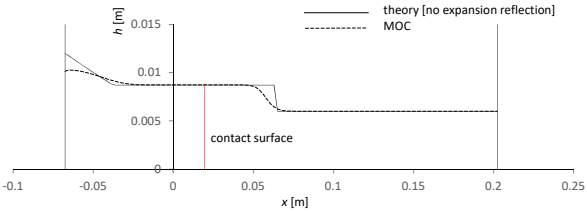

(c) t =0.196 [s] expansion to the left wall

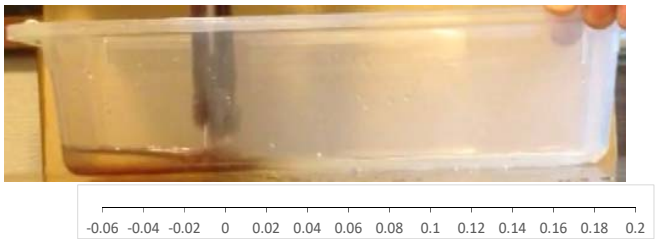

(c') time 01:12 t=0.18 [s] expansion to the left wall

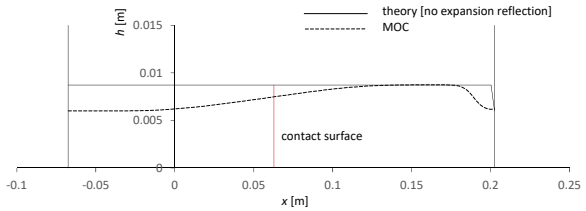

(d) t =0.621 [s] shock to the right wall

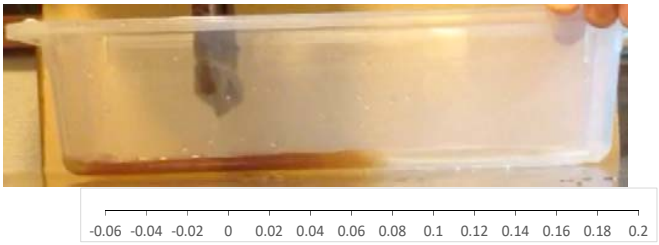

(d') time 01:56 t=0.62 [s] shock to the right wall

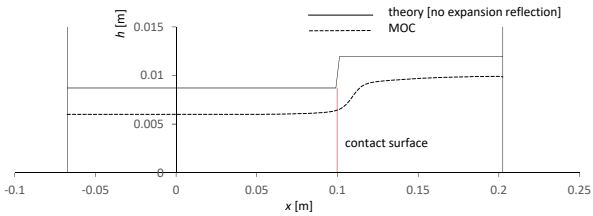

(e) time 01:96 t=1.02 [s] contact surface to shock $-0.0675 \le x \le 0.2025$ [m]

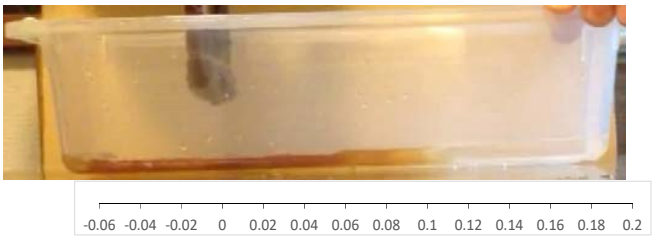

(e') t =0.996 [s] contact surface to shock $-0.0675 \le x \le 0.2025$ [m]

Fig. 26 Hydraulic Riemann problem (a)~(e): theory and MOC, (a')~(e'): experiment

ACKNOWLEDGMENT

The present author would like express thanks to Mr. D. Yamagishi for his experimental photos of circular cylinder and diamond airfoil.

REFERENCES

[1] A. H. Shapiro, *The Dynamics and Thermodynamics of Compressible Fluid Flow*, Vol. 1, 2, New York, John Wiley & Sons, 1953.
[2] H. W. Liepmann and A. Roshko, *Elements of as Dynamics,* New York, John Wiley & Sons, 1960.
[3] B. W. Imrie, *Compressible Fluid Flow*, London, Butterworths, 1973.
[4] S. Shreier, *Compressible Flow*, New York, John Wiley & Sons, 1982.
[5] M. Van Dyke, *An Album of Fluid Motion*, Stanford, CA, Parabolic Pr., 1982.
[6] J. D. Anderson, Jr., *Fundamentals of Aerodynamics*, New York, McGraw-Hills, 1991.
[7] M. A. Saad, *Compressible Fluid Flow*, Englewood Cliffs, Prentice-Hall, pp.337-348, 1993.
[8] M. H. Aksel and O. C. Erap, *Gas Dynamics*, Prentice-Hall, New York, 1994.
[9] J. D. Anderson, Jr., *Modern Compressible Flow: With Historical Perspective*, New York, McGraw Hills, 2004.
[10] W. J. Orlin, N. J. Lindner and J.G. Bitterly " Application of the analogy between water flow with a free surface and two-dimensional compressible gas flow," NACA Rep. No. 875, 1947, pp.311-328.
[11] J. E. Hatch, "The application of the hydraulic analogies to problems of two-dimensional compressible gas flow", M. Sc. Dissertation, Georgia School of Technology, March 1949.
[12] Y. Tomita, "A study of high speed gas flow by hydraulic analogy: The 4th report, flow around an airfoil", *Bulletin of JSME* vol.2, no.8, pp. 663-669, Nov 1959.
[13] V. Kumar, I. Ng, G. J. Sheard, K. Houriganand and A. Fouras, "Hydraulic analogy examination of under expanded jet shock cells using reference image topography," 8th International Symposium on Particle Image Velocimetry - PIV09, Melbourne, Victoria, Australia, August 25-28, 2009.
[14] P. K. Stansby, A. Chegini and T. C. D. Barnes, "The initial stages of dam-break flow," Journal of Fluid Mechanics, vol. 374, Nov.1998, pp. 407-424.
[15] T. Okada, T. Ishido and E. Morishita, "High-speed Aerodynamics and Shallow Water Theory (in Japanese)," Proceeding of JSME Kanto Branch Symposium, 2012(18), pp. 155-156, March 2012.
[16] E. Morishita, "Compressible pipe flow and water flow over a hump," Proceedings of the World Congress on Engineering 2013 Vol III, WCE 2013, July 3 - 5, 2013, London, U.K., 2013, pp.1739-1742.
[17] Y. Shimizu, "Non-uniform flow in open channel", Chapter 4, Lecture Note of Hydraulics (in Japanese), Hydraulic Research Laboratory, Hokkaido University, 2017.
[18] S. Awazu and K. Kimura, *Hydraulics Worked Examples* (in Japanese), Tokyo, Ohm, 1979, pp.255-256.
[19] I. H. Shames, *Mechanics of Fluids*, New York, McGraw-Hill, 1993, pp.739-745.
[20] I. A. Bedarev, A. V. Fedorov and V. M. Fomin, "Numerical analysis of the flow around a system of bodies behind the shock wave," Combustion Explosion and Shock Waves, vol.48, no.4, July 2012, pp 446–454.
[21] J. Sinclair and X. Cuia, "A theoretical approximation of the shock standoff distance for supersonic flows around a circular cylinder," Physics of Fluids, vol. 29, 2017, 026102-pp.1-13.

E. Morishita was born in Mie, Japan, August 26, 1949, with B.Eng. 1972, M. Eng. 1974, Dr. Eng. 1985 from the University of Tokyo together with M.Sc. 1983 from Cambridge (Hughes Hall). The author's major field of study is aerodynamics.

He worked for Mitsubishi Electric Corp. as Research Engineer to develop scroll compressor from laboratory to full scale production (1974-1987). He was Associate Professor and Professor of Aerodynamics (1987-2008) and Emeritus Professor (2010-present), the University of Tokyo. He then served as Professor of Mechanical Engineering in Utsunomiya University (2008-2015). Currently he is Part-Time Lecturer of Shibaura Institute of Technology and also Contract Professor of Mechanical Engineering, Meisei University, Tokyo, Japan. Previous publications include a book and an article "Spreadsheet Fluid Dynamics" (Tokyo, Maruzen, 2000 in Japanese/ J. Aircraft, 1999). Current research interests are aerodynamics education and applications including a traction flight vehicle called Cat Flyer.